Geomechanics and Engineering, *Vol. 19, No. 2 (2019) 105-114*
DOI: https://doi.org/10.12989/gae.2019.19.2.105

Distribution and evolution of residual voids in longwall old goaf

Changxiang Wang[1,2a], Ning Jiang[1,2], Baotang Shen*[1,2,4], Xizhen Sun[1,2], Buchu Zhang[1,2], Yao Lu[1,2] and Yangyang Li[1,2,3]

[1]College of Mining and Safety Engineering, Shandong University of Science and Technology, Qingdao 266590, China
[2]State Key Laboratory of Mining Disaster Prevention and Control Co-Founded by Shandong Province and the Ministry of Science and Technology, Qingdao 266590, China
[3]State Key Laboratory of Water Resource Protection and Utilization in Coal Mining, Beijing, China
[4]The Commonwealth Scientific and Industrial Research Organisation (CSIRO), PO Box 883, Kenmore, Queensland 4069, Australia

(Received November 1, 2018, Revised September 7, 2019, Accepted September 25, 2019)

Abstract. In this paper, simulation tests were conducted with similar materials to study the distribution of residual voids in longwall goaf. Short-time step loading was used to simulate the obvious deformation period in the later stage of arch breeding. Long-time constant loading was used to simulate the rheological stage of the arch forming. The results show that the irregular caving zone is the key area of old goaf for the subsidence control. The evolution process of the stress arch and fracture arch in stope can be divided into two stages: arch breeding stage and arch forming stage. In the arch breeding stage, broken rocks are initially caved and accumulated in the goaf, followed by the step deformation. Arch forming stage is the rheological deformation period of broken rocks. In addition, under the certain loads, the broken rock mass undergoes single sliding deformation and composite crushing deformation. The void of broken rock mass decreases gradually in short-time step loading stage. Under the water lubrication, a secondary sliding deformation occurs, leading to the acceleration of the broken rock mass deformation. Based on above research, the concept of equivalent height of residual voids was proposed, and whose calculation equations were developed. Finally, the conceptual model was verified by the field measurement data.

Keywords: longwall old goaf; residual voids; broken rock compression test; equivalent height of residual voids

1. Introduction

At present, the total area of coal mining-induced surface subsidence has reached 700,000 km^2 in China. As China's urbanization and industrialization accelerate, many large-scale construction projects (such as natural gas pipelines, factories, bridges, dams, high-rise buildings) are to be built on or pass through the old goafs of previously mined panels. As a result of coal mining, a variety of cavities and cracks are formed between broken rocks in the goaf (Shen and Barton 2018, Barbato *et al.* 2016, Ghabraie *et al.* 2015). The residual voids and the activation of voids in goaf are one of causes for the secondary subsidence, spontaneous combustion of coal seam, accumulation of harmful gas, water inrush of mine and so on (Sun *et al.* 2017, Salmi *et al.* 2017, Zhang *et al.* 2019). Under the load of surface building and the action of groundwater, the movement of the broken rock in the goaf can be activated again, resulting in additional deformation of the ground surface and hence building settlement, local cracking, tilt and even collapse. This seriously affects the planning, construction and safe operation of buildings above the goaf (Sasaoka *et al.* 2015, Xu *et al.* 2014, Wang *et al.* 2018).

To improve the suitability of goaf areas for construction, grouting has gradually become a mainstream method. For example, fly ash and cement are widely used as filling materials in coal mine backfill. Filling materials can strengthen the caving rock and support the overlying strata to reduce the surface subsidence (Jiang *et al.* 2017, Shen *et al.* 2017). Based on the study of key stratum theory, it is proved that the separation gap mainly appears under the key stratum which is a component rock layer that often halts the progressive deformation upwards. The dynamic evolution of the separation has been revealed, providing a theoretical basis for the design of grouting anti-sinking drilling (Xuan *et al.* 2017). Using grout injection into the horizontal fractures at the bed separation, the main injection section was located between the bottom of the injection borehole and the key stratum immediately above (Xuan *et al.* 2015).

As the working face continues to advance, overburden structures induced by mining continue to expand. The mining-induced overburden structures, i.e., a breaking arch. The weight of fractured rock layers in breaking arch is the loading source of the broken rock mass in goaf. The distribution of void in mining is closely related to the evolution of breaking arch (Rezaei *et al.* 2015, Wang *et al.* 2015). Overburden damage in coal mining is limited in its vertical extent because of the volume expansion of the roof material on fragmentation when bulkling-controlled caving occurs (Yavuz *et al.* 2004, Ma *et al.* 2017, Li *et al.* 2018). The stress-strain equation put forward by Salamon(1990)

*Corresponding author, Ph.D.
E-mail: Baotang.Shen@csiro.au
[a]Ph.D.
E-mail: 1554624100@qq.com

http://www.techno-press.org/?journal=gae&subpage=7
ISSN: 2005-307X (Print), 2092-6219 (Online)

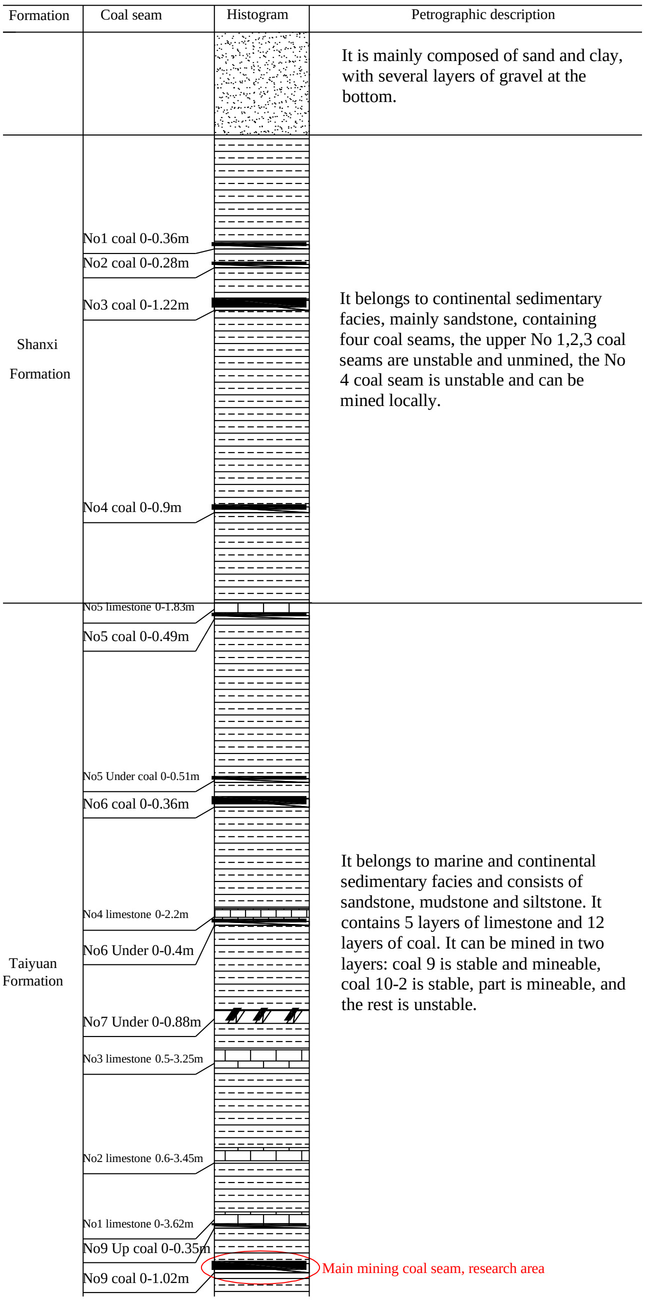

Fig. 1 Stratigraphic occurrence

described the compressive behaviour of caved rock in the gob has been utilized in the current study to fit the strain-hardening behaviour of backfill material sample. A large number of research results show that the shapes of rock blocks of various sizes produced by rock mass fragmentation have self-similarity. a model for predicting the void volume of falling gangue can be established by using Fractal Theory(Mondal *et al.* 2017; Ma *et al.* 2019).

In previous literature, in-depth studies on the goaf residual void and goaf gap treatment methods have been investigated. However, there are more qualitative analysis on the residual voids in goaf, and these results are difficult to be effectively applied to the field of goaf treatment. The compression of gangue in the laboratory was usually performed by the linear loading without considering filling water. Besides, the compression instrument has a limited size. To this end, based on the data of goaf treatment in China, similar simulation tests and broken rock compression tests are conducted by large compression instruments in this paper. The distribution of residual voids in longwall old goaf was studied, providing a reliable theoretical basis for the old goaf filling treatment.

2. Distribution of residual voids in long wall goaf

2.1 Background

The goaf of Shengjing Coal Mine is located in Zhangqiu, Jinan, Shandong Province, the main coal-bearing strata in Shengjing Coal Mine are Taiyuan formation and

Table 1 Mining status of coal seams

Coal seams	Average mining thickness/m	Coal-mining method	Coal-mining technology	Roof management method
No. 4	0.67	Tunnel mining	Blasting mining	Caving method
No. 9	1.09	Longwall mining		

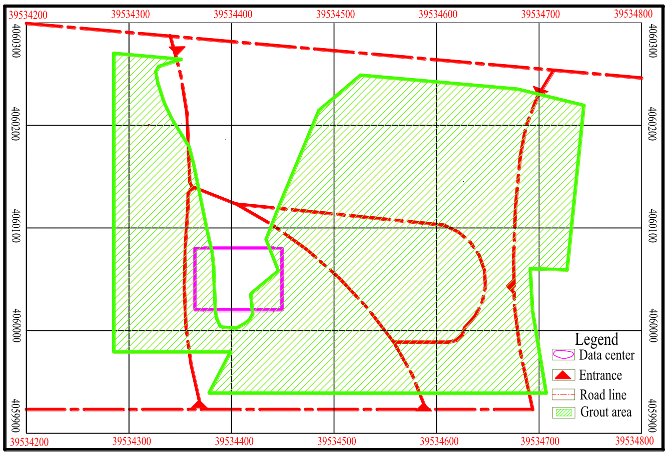

Fig. 2 Data center position and goaf distribution

Table 2 Characteristics of strata and model ratios

Strata number	Lithology	Depth of stratum/cm	Stratification thickness/cm	Number of replication	Proportion	Unit weight (g/cm^3)
R12	Quaternary	5.00	2.50	2	8:6:4	1.50
R11	Mudstone	9.00	1.50	6	8:6:4	1.50
R10	Sandstone	1.00	1.00	1	7:8:2	1.60
R9	No.4 coal	0.45	0.45	1	8:6:4	1.50
R8	Mudstone	1.00	1.00	1	8:6:4	1.50
R7	Sandstone	2.50	2.50	1	7:8:2	1.60
R6	Mudstone	15.00	3.00	5	8:6:4	1.50
R5	Sandstone	5.00	2.50	2	7:8:2	1.60
R4	Mudstone	25.00	2.50	10	8:6:4	1.50
R3	No.4 lime	1.00	1.00	1	8:6:4	1.50
R2	Fine sandstone	1.50	1.50	1	7:8:2	1.60
R1	Mudstone	1.50	0.75	2	8:6:4	1.50
M	No.9 coal	0.55	0.55	1	8:6:4	1.50
F1	Sandstone	5.00	2.50	2	7:8:2	1.60

Shanxi formation, as shown in Fig. 1. There are 13 layers of coal, and the total thickness of coal seams is 3.5 m. There are No.7 coal, No.9 coal, No.10-2 coal in Taiyuan formation, No.3 coal and No.4 coal in Shanxi formation.

A new E-commerce Industrial Park is planned to be distributed in the goaf of Shengjing Coal Mine, as shown in Fig. 2. To keep the constant indoor temperature and humidity, no deformation joints are allowed. Therefore, grouting is adapted to ensure the safety of the data processing center. At the same time, the distribution and evolution characteristics of voids in the goaf should be carefully analyzed to improve the grouting efficiency. The main coal seams in goaf are No. 4 and No.9 coal seams. The mining situations of these coal seams are shown in Table 1. No. 9 coal seam is extracted through the longwall mining with the average buried depth of about 160 m, while the average depth of No.4 coal is about 40 m. Thus, the mining influence of No. 4 on No. 9 coal seam is limited and can be ignored. The thickness of No. 9 coal seam mining areas in the working area is 0.68 ~ 1.13 m, with the average of 1.09 m.

2.2 Testing procedures

A plane strain model of 1.9 m ×1. 6m × 0.22 m is used in the similar simulation experiment test. According to the

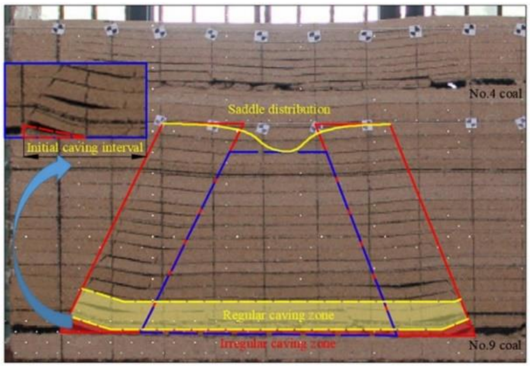

Fig. 3 Model after coal seam mining

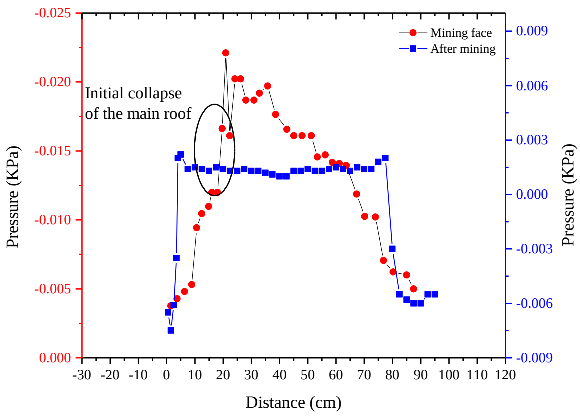

Fig. 4 Monitoring stress data of similar simulated stress

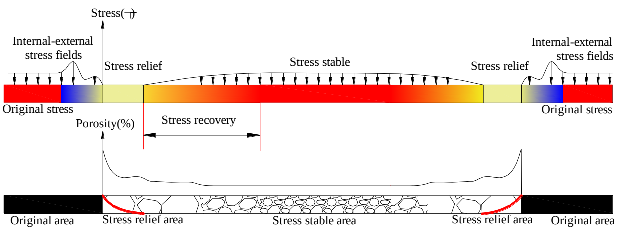

Fig. 5 Stress and void distribution models of stope (Song 1988, Wang 2017, Jaouhar *et al.* 2018)

principle of similarity simulation, the geometric similarity constant is 1: 200, the time similarity constant is 1: 14, and the bulk density similarity constant is 1: 1.5. According to the similarity condition, the proportion of sand, calcium carbonate and gypsum in the similar material is determined, and the amount of each layered material in the model is calculated. Considering the material loss during the laying process, the mass loss coefficient is 1.2, as shown in Table 2.

In this paper, the conventional method is used to mine No. 4 coal seam first and then the No. 9 coal seam. This paper only focuses on the void development after mining in the No. 9 coal seam. The stress of coal mining is observed by the micro pressure sensor of resistance strain after the mining of No. 9 coal. One sensor is placed at intervals of 5 cm in the center line of the No. 9 coal seam floor.

Stress data are positive for stress release and negative for stress concentration in Fig. 4. The red stress data is the stress when the working surface is advanced to a certain position, and the blue stress is the stress at each position of the stope after mining. In the similarity simulation test, the horizontal distance is 100 cm and the geometric similarity ratio is 1 :200, so the horizontal distance is 200 m in stope.

2.3 Void distribution in mining

2.3.1 Simulation results of void distribution in mining

Fig. 3 shows the mined model after a month, it can be seen that a middle trapezoid compaction zone and two parallelogram fracture zones at two sides of the compaction zone are formed, and fractures at top of the compaction zone are the saddle-shaped distribution pattern, the initial collapse step distance is about 34 m, and the periodic collapse step distance is about 12 m.

An approximately right triangle structure is formed near the cut-off hole and stopping line in the caving zone. The fracture tends to be closed without obvious breakage in regular caving zone during mining. The height of irregular caving zone is approximately equal to the mining thickness, forming a stable structure with relatively large voids, which are consistent with previous experimental description (Guo *et al.* 2001).

Horizontal fractures and vertical fractures are involved in the fracture zones, in which most fractures are closed in the mining advancing process, only a few fractures remain open. Over time, the fracture zone is further compressed and closed. The expansion coefficient of fractured zone can be considered as 0.

The results of stress monitoring in similar simulation tests are shown in Fig. 4. The stress evolution shows the zonal characteristic. In the early stage of mining, the stress rises slowly. When the mining advances to the first collapse of the roof, the stress increases obviously, then it reaches to be stable and decreases slowly. when the full mining is advanced, the decreasing speed is accelerated.

As shown in Fig. 4 and Fig. 5, the stress caused by collapse and compaction of the roof rock in the goaf are different. The stable goaf can be classified into the stress release area, stress recovery area and stress stable area. Stress stable area almost occupied all the space in the goaf. The stress state of the goaf stress stable area has experienced the stress release period, stress recovery period and stress stable period.

The stress release areas are situated in the two ends of the open-off-cut and finishing lines in goaf, which are not sufficiently collapsed, cannot withstand the pressure of the overlying strata. The closer distance to the middle of the goaf, the more frequent occurrence of rock collapse. Because of the bending and sinking action of the overlying strata, the caved rock is gradually compacted, forming a stress recovery area. The stress stable area is situated in the middle of the goaf where the caving rock is the most compacted.

2.3.2 Stress state evolution law of the stress arch

According to previous studies (Poulsen and Adhikary *et al.* 2018, Majdi and Hassani *et al.* 2012), the distribution of mining void is closely related to the evolution of stress and breaking arch. The stress arch and breaking arch in stope structure follow a dynamic evolution process in goaf, and it can be divided into the following two stages, three periods.

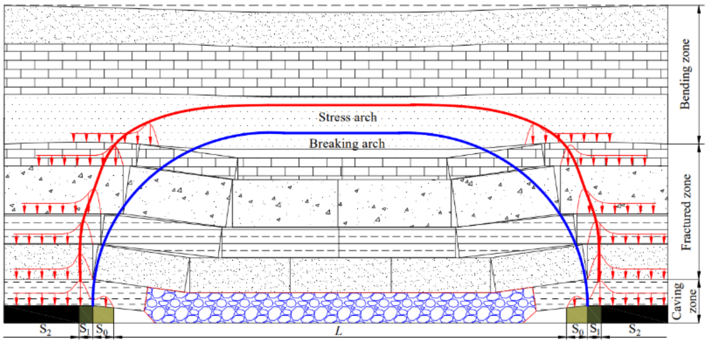

Fig. 6 Mechanics model of stope structure (S0 is the internal stress field; S1 is the plastic zone; S2 is the elastic zone)

The first stage is the arch breeding stage, i.e., stress release and stress recovery period of broken rock in goaf.

During the earlier arch breeding stage, i.e., the stress release period of broken rock in goaf, the overlying strata in goaf are separated along the interfaces, and the falling rock layer has not filled up the goaf. The fractured rock mass is accumulated, but free space still exists to be filled in the goaf. In addition, there is also a space to be compressed between the broken rock mass. At this stage, the goaf does not bear the pressure of overlying strata, all of which are stress release areas.

During the later arch breeding stage, i.e., the stress recovery period of broken rock in goaf, the falling rock has almost filled up the goaf. Since there is limited space, overburden strata above the falling rock cannot collapse into the goaf but lives in a state of fractured strata. The fractured strata rest on the falling broken rock mass. At this stage, only space among broken rocks in goaf can be compressed. Simultaneously, the broken rock deforms under the high pressure from the fractured strata. The area of stress release area in goaf decreases gradually, and the area of stress recovery area first increases and then decreases. The stress stable area increases gradually.

The second stage is arch forming stage, i.e., stress stable period of broken rock in goaf.

As shown in Fig. 6, the arch forming stage is also the stress stable period of broken rock in goaf. The range of stress recovery area is almost zero, the span of stress release area is about half of the initial collapsed distance of the immediate roof, and the overlying rock is fully deformed. The broken rock exhibits continuous strong rheological characteristics under high bearing pressure.

3. Experimental study on void evolution of broken rock

Similar simulation tests show that irregular caving zones can form stable structures with a large number of voids in similar simulation tests. The goaf deformation is mainly caused by the compressive deformation of broken rock mass in irregular caving zone. Hence, it is necessary to further study the characteristics of void evolution of broken rock to guide the in-situ grouting work. The experimental control system consists of a console and a servo loading system. The whole process is automatically controlled by the computer, experimental loading and unloading system and experimental preparation process, as shown in Fig. 7. The diameter of the test chamber is 400 mm and the height of the test chamber is 680 mm.

Fig. 7 Experimental system and experimental preparation process

3.1 Test schemes for void evolution of broken rock

Through similar simulation tests, it can be concluded that the weight of rock layer in breaking arch is the source of compression force for the broken rock in goaf. The force magnitude is directly related to the height of falling rock, increasing with the increase of fractured strata height. During the later stage of arch breeding, in the interval between two roof breakings, the pressure acting on the falling rock is basically unchanged, which is similar to the deadweight of the overlying breaking rock layer. When the roof is broken again, the pressure acting on the falling rock increases rapidly and the increment is approximately equal to the deadweight of the new broken overlying strata. Therefore, the stress state of falling rock in goaf is not increased in a linear way, but a ladder-type increasing trend. Therefore, the short-time step loading is adopted in the broken rock compression test.

The axial loads are set as 100kN, 200kN, 300 KN, 400KN, 500 KN, the loading rate is 0.5kN/s. The axial load in each level is maintained for 2.5 hours to simulate the multiple fracture phenomena in the later arch breeding stage. In particular, the influence of compression time on the compressive deformation of broken rock mass is obtained by maintaining the axial load of 500kN for 1. 25

hours.

Water effect is also considered in the simulation of the real goaf condition. The rise of groundwater level and seasonal precipitation lead to changes of the fractured rock, thus affecting the compressive deformation of fractured rock. Therefore, water is injected into the experimental cabin after maintaining the axial load of 500kN for 1. 25 hours. In this test, water just soak the fractured rock, but cannot generate much water pressure. The creep experiment is performed under water immersion to simulate the rheological deformation of the arch forming stage.

Talbot grading (Talbot and Richart. 1923) has important implications for the design of material proportion. The Talbot formula is defined as

$$p = 100\left(\frac{d}{D}\right)^n \tag{1}$$

where d is a certain particle size; p is the pass percentage of particles with radius smaller than d; D is the maximum grain size of the material, n is the Talbot coefficient, smaller than 1.

Results show that, with the Talbot's grading, gangue samples have a higher deformation modulus than fully graded and single-graded gangue samples, this feature can be used to simulate the compressive deformation of fractured rock mass in old goaf (Li *et al.* 2016). The maximum particle size is 60 mm. Therefore, the large blocks of fractured gangues are crushed and sieved into a total of 6 particle size interval, including 0 ~ 10 mm, 10 ~ 20 mm, 20 ~ 30 mm, 30 ~ 40 mm, 40 ~ 50 mm and 50 ~ 60 mm by the grading. After the mixing, the initial density under different experimental indexes is measured. When Talbot index n=0.5, the fractured rock mass has the largest density, so the calculated grade is the gradation used in the experiment.

3.2 Experimental results of void evolution of the broken rock

Rock expansion indicates that the crushed rock volume will be larger than the original volume. The coefficient of expansion or porosity is usually used

$$K = \frac{V_1}{V_0} \tag{2}$$

$$P = \frac{V_1 - V_0}{V_1} = 1 - \frac{1}{K} \tag{3}$$

where K is the crushing expansion coefficient; V_0 is the intact rock volume; V_1 is the fractured rock volume; P is the porosity.

The experiment is carried out after the dry fractured rock samples are put into the experimental cabin and laid flatly. The relationships between the axial load and the axial deformation versus time are shown in Fig. 8, the curves of expansion coefficients and porosity versus time are shown in Fig. 9. The parameters used the test are shown in Table 3.

In the loading stage, with the increase of the axial load, the axial deformation of the fractured rock increases

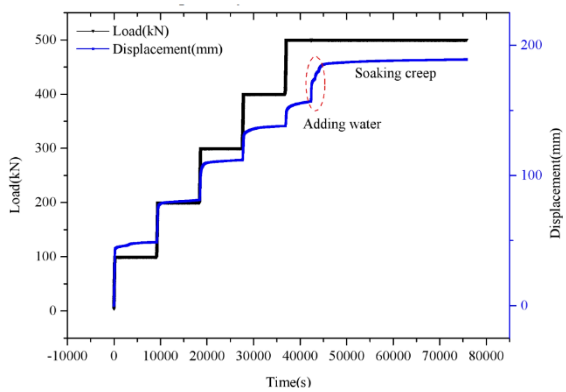

Fig. 8 Load and displacement

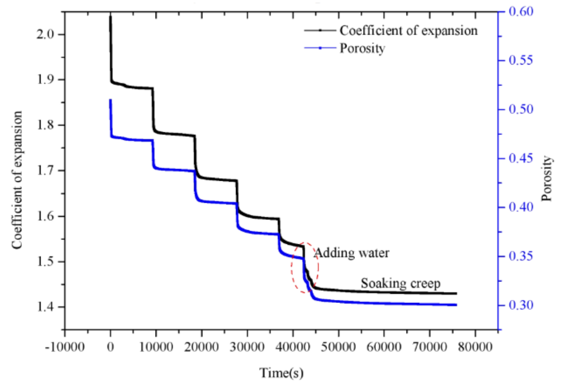

Fig. 9 Expansion coefficients and porosity

stepwise. When the 500kN load is maintained for 1.25 hours, the compressive deformation is 157.16mm. The coefficients of expansion and porosity show a decreasing trend. The expansion coefficient of the fractured rock reduces from 2.04 to 1.53 and the porosity reduces from 0.51 to 0.35.

During the test, the axial deformation of broken rock in loading stage is more obvious than that in the constant load stage. The axial deformation at each level exhibits logarithmic growth characteristics. The axial deformation increases rapidly at the initial stage of constant load, then decreases gradually, and tends to be stable at the end of constant load.

In the early stage of water injection, the axial deformation of fractured rock tends to increase sharply. With the increase of water quantity, the axial deformation of fractured rock shows an increasing trend with a decreasing rate. At the end of the injection stage, the axial deformation turns to the creep deformation with a logarithmic growth pattern. The creep test is maintained for about 7.75 hours, the compression amount is 188.79mm, fractured rock expansion coefficient decreases from 1.53 to 1.43, the porosity changes from 0.35 to 0.30 in the end of the soaking creep experiment.

3.3 Experimental analyses on void evolution of broken rock

3.3.1 Influence of load gradient on void evolution characteristics of broken rock

As shown in Figs. 10, 11 and Table 3, trends of axial

Table 3 Parameter variation of fractured rock during the test

Experimental stage	Deformation			Coefficient of expansion			Porosity		
	Initial/ mm	Final/ mm	Difference/mm	Initial	Final	Difference	Initial	Final	Difference
0-100kN Loading	0	41.77	41.77	2.04	1.90	0.14	0.51	0.47	0.04
100kN Constant load	41.77	48.70	6.93	1.90	1.88	0.02	0.47	0.47	0.00
100-200 kN Loading	48.70	72.18	23.48	1.88	1.81	0.07	0.47	0.45	0.02
200 kN Constant load	72.18	81.21	9.03	1.81	1.78	0.03	0.45	0.44	0.01
200-300 kN Loading	81.21	99.58	18.37	1.78	1.72	0.06	0.44	0.42	0.02
300 kN Constant load	99.58	111.80	12.22	1.72	1.68	0.04	0.42	0.40	0.02
300-400 kN Loading	111.80	125.02	13.22	1.68	1.64	0.04	0.40	0.39	0.01
400 kN Constant load	125.02	137.95	12.93	1.64	1.59	0.05	0.39	0.37	0.02
400-500 kN Loading	137.95	146.92	8.97	1.59	1.57	0.02	0.37	0.36	0.01
500 kN Constant load	146.92	157.16	10.24	1.57	1.53	0.04	0.36	0.35	0.01
Watering stage	157.16	173.39	16.23	1.53	1.48	0.05	0.35	0.32	0.03
Immersion creep stage（1.25h）	173.39	186.39	13.00	1.48	1.44	0.04	0.32	0.30	0.02
Immersion creep stage（7.75h）	186.39	188.79	2.40	1.44	1.43	0.01	0.30	0.30	0.00

Note: All values in the table are reserved for two decimal places

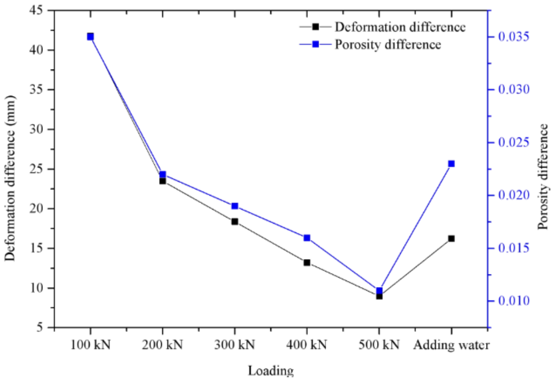

Fig. 10 Deformation and porosity change rates in the loading stage

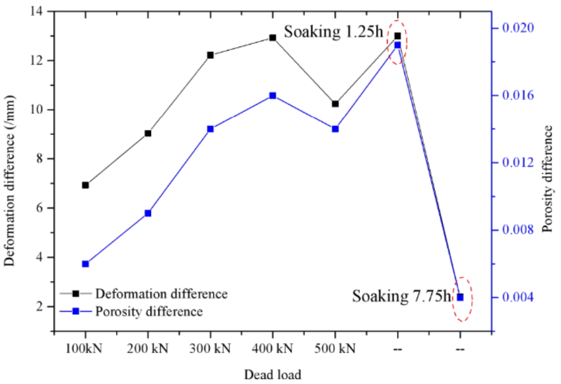

Fig. 11 Deformation and porosity change rates in constant load stage

compressive deformation and porosity are same in both the loading stage and the constant load stage, so the evolution characteristics of the porosity is mainly analyzed.

In the loading stage, with the increase of the load, the change rate of porosity decreases gradually. In the constant load stage, the porosity rate increases in the first four levels but decreases in the fifth level. This is because the fifth constant load stage is maintained for 1.25 hours, only half of the first four levels. Note also that the deformation value of the fifth constant load stage is 2.7mm less than that of the 400kN level, and the drop is only 20%, indicating that the loading time affects the porosity change rate.

At the initial stage of loading (mainly 0-100kN, 100-200kN), the sound of sliding friction between fractured rock blocks can be clearly heard, indicating that the fractured rock is undergoing a single sliding deformation. With the increase of load (mainly 200-300 kN, 300-400 kN, 400-500 kN), the sound of sliding friction decreases gradually, while the sound of rock fracture increase largely, indicating that the composite crushing deformation of broken rock occurs during the loading stage.

Through the above analyses, it can be concluded that single sliding deformation and composite crushing deformation occur in the broken rock mass under the loading action. The single sliding deformation of broken rock occurs in the early loading stage, mainly accompanying with the position adjustment. The friction between broken rock masses is mainly overcome. It can be seen from Fig. 8 that the deformation approximately shows a linear increasing trend in the loading stage at every loading stage.

Composite crushing deformation occurs when the load gradient increases to some extent. On one hand, it is caused by the increasing load, namely the broken rock mass are broken down into smaller block and subjected to sliding, filling, compacting. On the other hand, it is caused by the smoother broken rock mass. When the friction force decreases, the broken rock mass further slips, fills, compacts. At this stage, the void between the fractured rock mass is greatly reduced, and the accelerated deformation occurs.

The porosity phase difference of broken rock mass decreases gradually during the loading stage, indicating that the deformation in loading stage is dominated by the single sliding deformation. With the increase of load gradient, the sliding space becomes smaller. The difference of the void fraction in the stage of constant load increases gradually. This indicates that the composite fracture deformation is dominant in the constant load stage. And as the load gradient increases, the probability of fracture of the broken rock increases.

3.3.2 Influence of water on the characteristics of void evolution of broken rock

As shown in Fig. 10, Table 3, in the loading-watering stage, the porosity phase difference decreases first and then increases. With the increase of axial load, the porosity phase difference becomes smaller and smaller. When the pressure is 500kN, the porosity phase difference reaches the minimum value. At the same load, the watering stage just lasts for about 10 minutes, but the porosity phase difference is higher than that in the 500kN loading stage.

As shown in Fig. 11, Table 3, in the dead load - soakng stage, with the increase of axial load, the change rate of porosity follows the trend of increase-decrease-increase-decrease. Especially in the initial 1.25h stage of soaking load, the porosity change rate is much larger than that of other constant load stages, including that of the 100kN in the natural state.

Under the water lubrication, the secondary sliding deformation can be achieved under the constant load without undergoing the crushing deformation. Therefore, under the action of water, the void of broken rocks decreases sharply, and the deformation of broken rock is accelerated.

4. Engineering applications

In this paper, as shown in Fig. 12, the distribution law of residual voids in old goaf is obtained by similar simulation test, and the residual voidage in irregular collapse zone is obtained by broken rock compression test. On this basis, the concept of equivalent height of residual voids is put forward and verified by field grouting. The conclusion of this paper can provide theoretical basis for field grouting design.

4.1 Grouting range and porosity

The results of similar simulation tests show that the void of the fractured zone and regular caving zone can be neglected because of the closure effect of fracture. There are large voids caused by the different fracture forms in irregular caving zone, and it is difficult for large voids to be completely closed over time. Thus, these voids are the key areas of grouting treatment.

The height of the irregular caving zone is 0.92 ~ 0.98 times of the extracted thickness (Guo *et al.* 2001). The porosity of the stress stable area is determined by the compression test of broken rock discussed above in Section

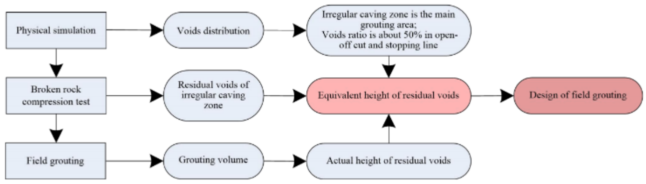

Fig. 12 Connections among physical simulation, void evolution test and field application

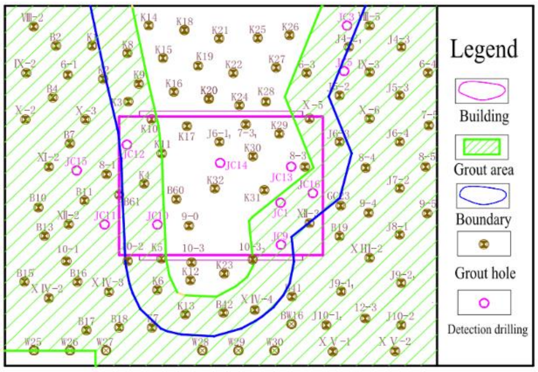

Fig. 13 Grouting holes and detection holes

3, the void ratio is 30%.

The stress release area forms an approximate right-angle triangle structure near the open-off cut and stopping line, so the void ratio is approximately 50%. The span of the stress release area is half of the initial collapse distance of the immediate roof, about 17 m.

4.2 Quantity Prediction of borehole grouting

4.2.1 Equivalent height of residual voids

To better guide the grouting in the field, the concept of the equivalent height of residual voids is put forward. Namely, the equivalent height of residual voids is defined as the product of the height of compacted broken rock to be treated by grouting and its void ratio in old goaf. Then, the equivalent height of residual voids can be calculated as

$$h_p = H_g * \varepsilon \tag{4}$$

where h_p is the equivalent height of residual voids in grouting region (m); H_g is height of strata treated by grouting (m); ε is the void ratio in the grouting area.

The height of the stress stabilization zone in irregular caving zone is 0.92 ~ 0.98 times of the mining thickness. The void ratio is 0.3, the equivalent height of residual voids is 0.30 m (the upper limit value is taken). The height of the stress release zone in irregular caving zone is approximate to the mining thickness, so the equivalent height of residual voids is 0.50 m.

4.2.2 Quantity prediction of single hole grouting

According to the concept of equivalent height of residual voids and the rule of this experiment, the quantity of single hole grouting can be estimated as

$$Q = S * h_p / C \tag{5}$$

where Q is the single hole grouting quantity (m^3); S is the single hole control area (m^2); C is the setting rate of grouting with value between 0.70~0.95, and here it is 0.9.

The grouting work can be guided by comparing the single hole grouting quantity with the actual grouting quantity. Besides, the sufficient grouting can be ensured without wasting grouting materials.

4.3 Analyses on the grouting quantity

As shown in Fig. 13, the total number of boreholes is 101. With 17m from the open-off cut as the boundary, the grouting holes are divided into the grouting holes in the stress release zone and stress stabilization zone. The grouting volume of the hole near the boundary line is counted as the half volume of the grouting hole. There are 27 grouting holes in the stress release zone. The controlled grouting area is 206.20 m^2, the grouting volume is 2810.70 m^3, the average grouting quantity is 104.10 m^3, and the equivalent height of residual voids is 0.45 m. There are 74 grouting holes in the stress stabilization zone with a controlled grouting area of 286.20 m^2 and a total grouting volume of 6682.20 m^3, with an average grouting volume of 90.30m^3, equivalent height of residual voids is 0.28 m.

5. Conclusions

Similar simulation shows that, the void ratio of the goaf varies greatly due to its randomness structure and the diversity of the mining conditions. Since the long wall goaf has experienced a long time compression process, the structure and the void ratio tends to be stable to a certain value. Because of the closure effect of fracture, grouting treatment is not necessary for the void in fracture zone and regular caving zone. Besides, the irregular caving zone is the key location.

• In each deformation process of broken rock in goaf, an obvious linear deformation exists in the early stage and the logarithmic creep deformation exists in the later stage. The broken rock in the natural state is gradually compacted, and the compressive deformation is gradually reduced. The above phenomenon corresponds to the subsidence rate of the ground surface decreases gradually and eventually tends to be stable.

• Under the influence of the loading gradient and water, the broken rock mass, which has become stable in the natural state, still has the rapid and obvious compressive deformation. Results show that the unsaturated broken rock mass in the goaf which has become stable still has the rapid and obvious compressive deformation after filling the water or under a building load, resulting in the secondary settlement of the surface above the goaf.

• To avoid the activation of broken rock in old goaf and reduce the void ratio, the grouting of broken rock void is essential in the old goaf. The concept of equivalent height of residual voids is proposed based on the similar simulation test, compression test of broken rock mass. The equation for estimating grouting quantity of single hole is further obtained and verified by the monitoring data in the field.

• From comparison of estimated grouting volume and actual grouting volume, it is found that the equivalent height of residual voids, the equivalent height of residual voids is estimated to be slightly larger. This indicates that, broken rocks are affected by various factors in the real environment, such as the weight of overburden rocks, the combined characteristics of lithology, rock particle size gradation and water. The old mined-out broken rock is compressed more intensively with lower void ratio.

Acknowledgments

This work was supported by Shandong Provincial Natural Science Foundation (ZR2019BEE013); Key Research and Development Plan of Shandong Province(2018GSF120003) and National Natural Science Foundation of China (51804179, 51974173); Taishan Scholar Talent Team Support Plan for Advantaged & Unique Discipline Areas, the graduate student science and technology innovation project of Shandong University of Science and Technology (SDKDYC190348).

References

Barbato, J., Hebblewhite, B., Mitra, R. and Mills, K., (2016), “Prediction of horizontal movement and strain at the surface due to longwall coal mining”, *Int. J. Rock Mech. Min. Sci.*, **84**, 105-118. https://doi.org/10.1016/j.ijrmms.2016.02.006.

Ghabraie, B., Ren, G., Zhang, X. and Smith, J. (2015), “Physical modelling of subsidence from sequential extraction of partially overlapping longwall panels and study of substrata movement characteristics”, *Int. J. Coal Geol.*, **140**, 71-83. https://doi.org/10.1016/j.coal.2015.01.004.

Guo, G. L., (2001). *Deformation Mechanism and Control of Building Foundation over Old Goaf*, China University of Mining and Technology Press, Xuzhou, China.

Jaouhar, E.M., Li, L. and Aubertin, M. (2018), “An analytical solution for estimating the stresses in vertical backfilled stopes based on a circular arc distribution”, *Geomech. Eng.*, **15**(3), 889-898. https://doi.org/10.12989/gae.2018.15.3.889.

Jiang, N., Zhao, J., Sun, X., Bai, L. and Wang, C. (2017), “Use of fly-ash slurry in backfill grouting in coal mines”, *Heliyon*, **3**(11), e00470. https://doi.org/10.1016/j.heliyon.2017.e00470.

Kim, S.M. and Choi, Y. (2018), “SIMPL: A simplified model-based program for the analysis and visualization of groundwater rebound in abandoned mines to prevent contamination of water and soils by acid mine drainage”, *Int. J. Environ. Res. Public Health*, **15**(5), 951. https://doi.org/10.3390/ijerph15050951.

Li, M., Zhang, J. and Gao, R. (2016), “Compression characteristics of solid wastes as backfill materials”, *Adv. Mater. Sci. Eng.*, http://dx.doi.org/10.1155/2016/2496194.

Li, X.S. and Xu, J.L. (2009), “A model of void distribution in collapsed zone based on fractal theory”, *Procedia Earth Planet. Sci.*, **1**(1), 203-210. https://doi.org/10.1016/j.proeps.2009.09.034.

Li, Y., Zhang, S. and Zhang, X. (2018), “Classification and fractal characteristics of coal rock fragments under uniaxial cyclic loading conditions”, *Arab. J. Geosci.*, **11**(9), 201-212. https://doi.org/10.1007/s12517-018-3534-2.

Ma, D., Duan, H., Liu, J., Li, X. and Zhou, Z. (2019), “The role of gangue on the mitigation of mining-induced hazards and environmental pollution: An experimental investigation”, *Sci.*

Total Environ., **664**, 436-448. https://doi.org/10.1016/j.scitotenv.2019.02.059.

Ma, D., Rezania, M., Yu, H. and Bai, H. (2017), "Variations of hydraulic properties of granular sandstones during water inrush: Effect of small particle migration", *Eng. Geol*., **217**, 61-70. https://doi.org/10.1016/j.enggeo.2016.12.006.

Majdi, A., Hassani F.P. and Nasiri, M.Y. (2012), "Prediction of the height of destressed zone above the mined panel roof in longwall coal mining", *Int. J. Coal Geol*., **98**, 62-72. https://doi.org/10.1016/j.coal.2012.04.005.

Mondal, D., Roy, P.N.S. and Behera, P.K. (2017), "Use of correlation fractal dimension signatures for understanding the overlying strata dynamics in longwall coal mines", *Int. J. Rock Mech. Min. Sci*., **91**, 210-221. https://doi.org/10.1016/j.ijrmms.2016.11.019.

Poulsen, B., Adhikary A.D. and Guo, H. (2018), "Simulating mining-induced strata permeability changes", *Eng. Geol*., **237**, 208-216. https://doi.org/10.1016/j.enggeo.2018.03.001.

Rezaei, M., Hossaini, M.F. and Majdi, A. (2015), "A time-independent energy model to determine the height of destressed zone above the mined panel in longwall coal mining", *Tunn. Undergr. Sp. Technol*., **47**, 81-92. https://doi.org/10.1016/j.tust.2015.01.001.

Salamon, M.D.G. (1990), "Mechanism of caving in longwall coal mining", *Proceedings of the Rock Mechanics Contributions and Challenges: Proceedings of the 31st US Symposium on Rock Mechanics,* Golden, Colorado, U.S.A., June.

Salmi, E.F., Nazem, M. and Karakus, M., (2017), "Numerical analysis of a large landslide induced by coal mining subsidence", *Eng. Geol*., **217**, 141-152. https://doi.org/10.1016/j.enggeo.2016.12.021.

Sasaoka, T., Takamoto, H., Shimada, H., Oya, J., Hamanaka, A. and Matsui, K., (2015), "Surface subsidence due to underground mining operation under weak geological condition in Indonesia", *J. Rock Mech. Geotech. Eng*., **7**(3), 337-344. https://doi.org/10.1016/j.jrmge.2015.01.007.

Shen, B. and Barton, N. (2018), "Rock fracturing mechanisms around underground openings", *Geomech. Eng*., **16**(1), 35-47. https://doi.org/10.12989/gae.2018.16.1.035.

Shen, B., Poulsen, B., Luo, X., Qin, J., Thiruvenkatachari, R. and Duan, Y. (2017), "Remediation and monitoring of abandoned mines", *Int. J. Min. Sci. Technol*., **27**(5), 803-811. https://doi.org/10.1016/j.ijmst.2017.07.026.

Song, Z.Q. (1988), *Practical Mining Pressure Control*, China University of Mining and Technology Press, Xuzhou, China

Sun, X., Yang, P. and Zhang, Z. (2017), "A study of earthquakes induced by water injection in the changning salt mine area, SW China", *J. Asian Earth Sci*., **136**, 102-109. https://doi.org/10.1016/j.jseaes.2017.01.030.

Talbot, A.N. and Richart, F.E. (1923), *The Strength of Concrete-its Relation to the Cement, Aggregates and Water*, University of Illinois at Urbana Champaign, Illinois, U.S.A.

Wang, C., Lu, Y., Cui, B., Hao, G. and Zhang, X. (2018), "Stability evaluation of old goaf treated with grouting under building load", *Geotech. Geol. Eng*., **36**(4), 2553-2564. https://doi.org/10.1007/s10706-018-0482-2.

Wang, L., Xie, G.X. and Wang, J.A. (2015), "Numerical investigation on the influence of surrounding rock stress shell on fractured field", *J. China Coal Soc*., **40**(9), 2009-2014.

Wang, W. (2017), "A analytical model for cover stress re-establishment in the goaf after longwall caving mining", *J. South. Afr. Inst. Min. Metall*., **117**(7), 670-683.

Xu, P., Mao, X., Zhang, M., Zhou, Y. and Yu, B. (2014), "Safety analysis of building foundations over old goaf under additional stress from building load and seismic actions", *Int. J. Min. Sci. Technol*., **24**(5), 713-718. https://doi.org/10.1016/j.ijmst.2014.03.030.

Xuan, D. and Xu, J. (2017), "Longwall surface subsidence control by technology of isolated overburden grout injection", *Int. J. Min. Sci. Technol*., **27**(5), 813-818. https://doi.org/10.1016/j.ijmst.2017.07.014.

Xuan, D., Xu, J., Wang, B. and Teng, H. (2015), "Borehole investigation of the effectiveness of grout injection technology on coal mine subsidence control", *Rock Mech. Rock Eng*., **48**(6), 2435-2445. https://doi.org/10.1007/s00603-015-0710-5.

Yavuz, H. (2004), "An estimation method for cover pressure re-establishment distance and pressure distribution in the goaf of longwall coal mines", *Int. J. Rock Mech. Min. Sci*., **41**(2), 193-205. https://doi.org/10.1016/S1365-1609(03)00082-0.

Zhang, S., Li, Y., Shen, B., Sun, X. and Gao, L. (2019), "Effective evaluation of pressure relief drilling for reducing rock bursts and its application in underground coal mines", *Int. J. Rock Mech. Min. Sci*., **114**, 7-16. https://doi.org/10.1016/j.ijrmms.2018.12.010.

GC